



# Cold-Formed Steel Built-Up I-Beam with the Trapezoidal Corrugated Web: Tests and Numerical Simulation

A. R. Dar<sup>1</sup> · M. Anbarasu<sup>2</sup> · G. Arun Kumar<sup>2</sup>

Received: 23 March 2021 / Accepted: 11 August 2021 / Published online: 15 September 2021  
© The Institution of Engineers (India) 2021

**Abstract** The use of cold-formed steel (CFS) sections as the primary load-carrying members in residential and industrial buildings is rising. Different forms of cross sections are adopted for flexural members. This article presents a detailed study on the flexural performance of CFS built-up flexural members with corrugated web. The influence of different parameters, such as the aspect ratio and angle of corrugation, towards evaluating the appropriateness of the current design methods in the design of cold-formed steel built-up I-beam with the trapezoidal corrugated web was assessed. Twenty-eight simply supported beam specimens under monotonically applied four-point bending were studied. A nonlinear finite element analysis (FEA) was also conducted by using ANSYS software, and the numerical models were validated against the test results. The FEA results were in close agreement with that of the experiment. Further, the experimental as well as the numerical flexural strengths of specimens were compared with the design strengths predicted by using North American Specifications (AISI S100-2007) and Australian/New Zealand standards (AS/NZ: 4600-2005) for cold-formed steel structures. The current design specifications were assessed by conducting a reliability analysis. The comparison of the results shows that the corrugation angle and aspect ratio have a significant influence on the flexural capacity of beams.

**Keywords** Aspect ratio · Cold-formed steel beams · Corrugation angle · Lipped I-section · Trapezoidal corrugation

## Abbreviations

$a$	Plane length of flat panel
$b$	Projection length of the inclined
$b_f$	Breadth of the flange
$b_l$	Length of the lip
$c$	Length of the inclined panel
$d$	Depth of corrugation
$d_{\max}$	Maximum depth of corrugation
$E$	Young's modulus
$f_{oy}$	Elastic buckling stress for flexural buckling about the $y$ -axis and
$f_{oz}$	Elastic buckling stress for torsional buckling
$f_y$	Yield stress
$f_u$	Ultimate stress
$h_w$	Height of the web
$L$	Length of the specimen
$M_{\text{Exp}}$	Experimental moment capacity
$M_{\text{FEA}}$	Moment capacity predicted by FEA
$M_{\text{AISI}}$	Moment capacity predicted by North American Specifications (AISI S100-2007) and
$M_{\text{AS/NZ}}$	Moment capacity predicted by Australian/New Zealand standards (AS/NZ: 4600-2005)
$t_f$	Thickness of the flange
$t_l$	Thickness of the line
$t_w$	Thickness of the corrugated web
$\beta$	Aspect ratio
$\nu$	Poisson's ratio
$\theta$	Corrugation angle

✉ M. Anbarasu  
gceanbu@gmail.com

<sup>1</sup> Department of Civil Engineering, National Institute of Technology Srinagar, Srinagar, Jammu & Kashmir 190006, India

<sup>2</sup> Department of Civil Engineering, Government College of Engineering, Salem, Tamil Nadu 636 011, India

## Introduction

The utilization of cold-formed steel sections is increasing all over the world in the construction of residential and industrial buildings due to their advantages over hot-rolled sections. Different sections, such as channel and Z sections, are commonly used as purlins and girt in roof and wall systems, in which these members are used as the secondary load-carrying members. Nowadays, CFS sections are also used as the primary load-carrying members through modification of cross sections, built-up sections and other methods of forming. Such members' strength and stability depend on the cross-sectional dimensions of the geometry and the overall slenderness as a member [1, 2]. For the inexpensive design of flexural member, a slender web may be sufficient to transmit the shear, whereas the flanges support external loads by using a greater part of the material. But the flat web has the possibility of occurrence of buckling in the compression zone before yielding, which requires further studies towards improving the strength of the web. The issue is overcome by using a corrugated web as an alternative to the plane web, which produces superior strength and stability without additional thickness and stiffeners with lesser thickness [3–7].

Sherman and Fisher [8] investigated the connection between the corrugated web and flange in beams and concluded that the longitudinal weld only is effective to resist the slip between web and flange. Lindner [9] studied the lateral–torsional buckling behaviour of steel girders with corrugated webs through experiments and established that the warping constant is different for the corrugated web beam compared to the beam with flat web. Luo and Edlund [10] assessed various factors that influence the ultimate strength of girders with trapezoidal corrugation under patch loading. Elgaaly et al. [11–13] investigated the bending and shear behaviour of corrugated webs under uniform bending and concluded that for design, the ultimate moment capacity is dependent on the flange yielding, and design equations were also proposed for corrugated web beams. Khalid et al. [14] investigated the behaviour of beams with corrugated web subjected to a three-point bending and concluded that the moment-carrying capacity of vertical corrugated web beam is higher than that of a horizontal corrugated web beam. Sayed-Ahmed [15] reported that the post-buckling strength of the girder with the corrugated web is extremely dependent on the panel width of the corrugations. Abbas et al. [16] investigated the transverse flange bending of I-girder with corrugated web and analysed in-plane bending behaviour of corrugated web I-girder using the conventional beam theory, whereas

out-of-plane torsional behaviour was analysed as a flange transverse bending problem for calculating the primary moment and shear. Sayed-Ahmed [17] studied the design aspects of steel I-girders with corrugated webs and established that the lateral–torsional buckling resistance is higher than plate girder with plane web and found that the equations used to calculate the critical moment of girders with plane webs would undervalue the strength of the plate girders with web corrugation, but conservative for design purposes.

Moon et al. [18, 19] have proposed an interactive shear buckling coefficient and shear buckling parameter for corrugated steel webs and investigated the lateral–torsional buckling of I-girder with corrugated web under uniform bending. He et al. [20] have presented state-of-the-art mechanical behaviour of the composite bridges with corrugated steel webs. Nagy et al. [21] developed a frame made of CFS beams with corrugated web and square hollow section (SHS) columns and demonstrated with good structural performance. Dubina et al. [22, 23] reported the experimental behaviour of a built-up beam consisting of cold-formed steel sheets and flanges of built-up cold-formed steel members (back-to-back lipped channels) with trapezoidal webs made with self-drilling screws. Ballok [24] reported experimental behaviour and modes of trapezoidal beams made of cold-formed steel profiles and corrugated web-based tests constructed at the Technical University of Cluj-Napoca.

The lack of available literature on the effects of aspect ratio and corrugation angle of trapezoidal corrugation on the flexural capacity of CFS I-beam with the corrugated web is scarce. In view of this, this paper presents the details of the performance studies conducted on the buckling behaviour, and flexural capacity of CFS lipped I-beam with trapezoidal corrugated web. A total of 28 simply beams was tested under four-point bending about the major axis of the sections by varying the aspect ratio of corrugation. Out of 28 specimens, seventeen specimens were tested by varying the aspect ratio for three series of lengths 1800, 3000 and 3600 mm. The remaining eleven specimens were studied for their performance by varying the corrugation angle for two series of length of 3000 and 3600 mm. The flexural capacity and corresponding deformed failure modes at ultimate moments were obtained. In addition, nonlinear shell finite element analysis (FEA) was also carried out by using ANSYS [25] general-purpose software by incorporating material and geometric nonlinearities. The appropriateness of the current North American Specifications [26] and Australian/New Zealand standards [27] was evaluated for all the specimens.

## Experimental Investigation

### Test Specimens

The test specimens were fabricated from locally available CFS sheets. CFS sheets of 2 mm thick were used for flanges and 1.2 mm for the web. Flanges and web were connected by spot weld at the nodal points. Figure 1 shows the details of the lipped cold-formed I-beam with the corrugated web.

Stiffeners of 3-mm-thick CFS sheets were provided at the loading points and supports to avoid the bearing failure near the supports and to uniformly distribute the load at the loading points. The test specimens were designated as “ $L-d_w-b_f-a/b-\theta$ ”, in which  $L$ ,  $d_w$ ,  $b_f$ ,  $a/b$  and  $\theta$  denote span, depth of the web, width of flange, aspect ratio and corrugation angle, respectively (Example in 3000-300-100-0.5-45). The aspect ratio,  $a/b$ , is the ratio of the length of horizontal panel to the inclined panel of trapezoidal corrugation. The corrugation angle is the angle made by the inclined panel with the horizontal panel. The average

measured dimensions of the test specimens are presented in Table 1.

The material properties of CFS sheet were obtained by conducting tensile coupon tests according to the Indian Standard [28]. The coupons were extracted from the parent steel sheet for the respective thickness. The material properties obtained from the coupon test are presented in Table 2. Figure 2 shows the typical view of the stress–strain curve of 2-mm-thick CFS sheet. The residual stresses were not measured, as both the flexural and membrane residual stresses tend to be insignificant compared with the yield stress in specimens made by using the press-braking process [29].

### Experimental Set-up

The experimental investigations had been carried out for all the specimens in a 500-kN loading frame. The typical view of the experimental set-up and schematic diagram are shown in Figs. 3 and 4, respectively.

**Fig. 1** Details of lipped I-beam with corrugated web

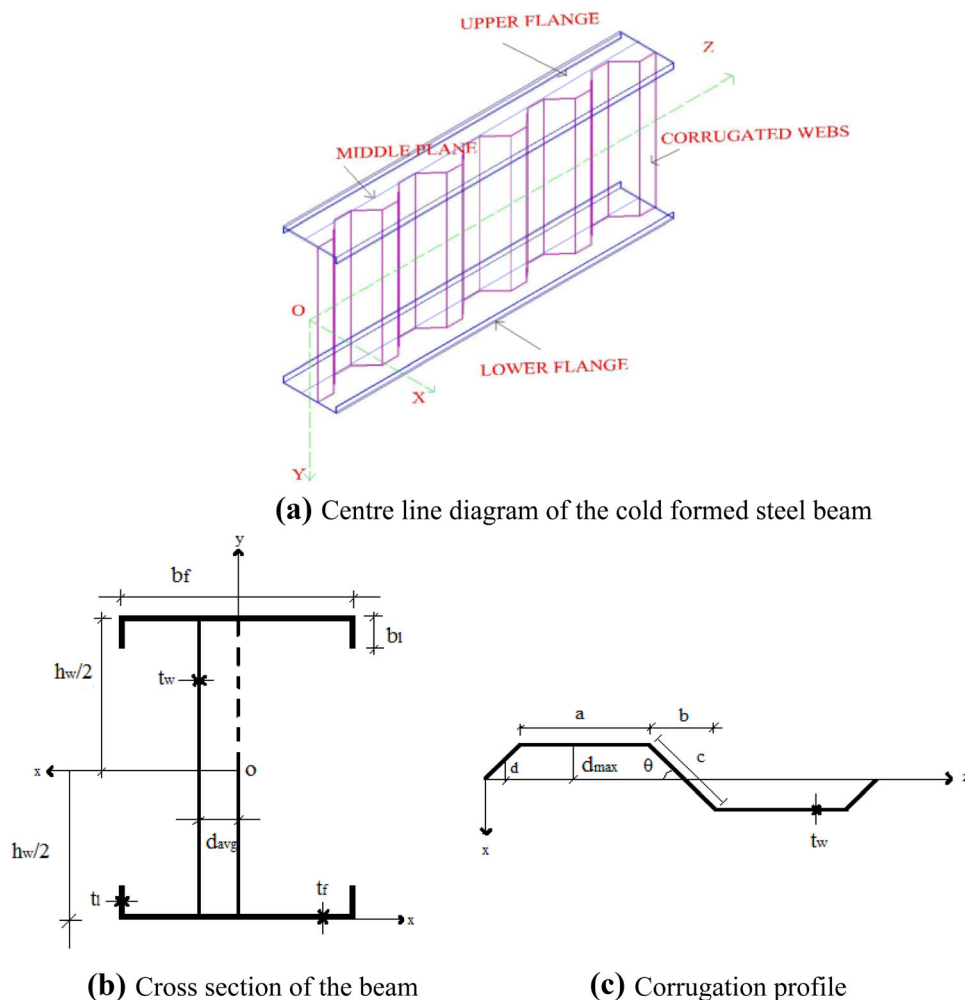


**Table 1** Average measured dimension of the test specimens

Specimen ID	$a$ (mm)	$b$ (mm)	$c$ (mm)	$d_{\max}$ (mm)	$\theta$	$t_w$ (mm)	$h_w$ (mm)	$b_f$ (mm)	$t_f$ (mm)	$b_l$ (mm)	$t_l$ (mm)	$L$ (mm)	Aspect ratio ( $\beta$ )
3000-300-100-0.5-45	60	80.0	113.1	40.0	45	1.2	300	100	2	15	2	3000	0.5
3000-300-100-0.7-45	60	60.0	84.8	30.0	45	1.2	300	100	2	15	2	3000	0.7
3000-300-100-1.1-45	60	40.0	56.6	20.0	45	1.2	300	100	2	15	2	3000	1.1
3000-300-100-2.1-45	60	20.0	28.3	10.0	45	1.2	300	100	2	15	2	3000	2.1
3600-400-150-0.5-45	60	84.8	120.0	42.4	45	1.2	400	150	2	15	2	3600	0.5
3600-400-150-1.0-45	60	42.4	60.0	21.2	45	1.2	400	150	2	15	2	3600	1.0
3600-400-150-1.5-45	60	28.3	40.0	14.1	45	1.2	400	150	2	15	2	3600	1.5
3600-400-150-2.0-45	60	21.2	30.0	10.6	45	1.2	400	150	2	15	2	3600	2.0
1800-200-100-0.5-45	20	28.3	40.0	14.1	45	1.2	200	100	2	15	2	1800	0.5
1800-200-100-1.0-45	40	28.3	40.0	14.1	45	1.2	200	100	2	15	2	1800	1.0
1800-200-100-2.0-45	40	14.1	20.0	7.1	45	1.2	200	100	2	15	2	1800	2.0
1800-200-100-3.0-45	60	14.1	20.0	7.1	45	1.2	200	100	2	15	2	1800	3.0
1800-300-100-0.5-45	60	84.8	120.0	42.4	45	1.2	300	100	2	15	2	1800	0.5
1800-300-100-1.0-45	60	42.4	60.0	21.2	45	1.2	300	100	2	15	2	1800	1.0
1800-300-100-2.0-45	60	21.2	30.0	14.1	45	1.2	300	100	2	15	2	1800	2.0
1800-300-100-3.0-45	180	42.4	60.0	21.2	45	1.2	300	100	2	15	2	1800	3.0
1800-300-100-4.0-45	240	42.4	60.0	21.2	45	1.2	300	100	2	15	2	1800	4.0
3000-300-100-1.0-15	60	57.9	60.0	7.7	15	1.2	300	100	2	15	2	3000	1.0
3000-300-100-1.0-30	60	51.9	60.0	15.0	30	1.2	300	100	2	15	2	3000	1.0
3000-300-100-1.0-45	60	42.4	60.0	21.2	45	1.2	300	100	2	15	2	3000	1.0
3000-300-100-1.0-60	60	30.0	60.0	25.9	60	1.2	300	100	2	15	2	3000	1.0
3600-400-150-Flat web	60	–	–	–	0	1.2	400	150	2	15	2	3600	–
3600-400-150-1.0-15	60	57.9	60.0	7.7	15	1.2	400	150	2	15	2	3600	1.0
3600-400-150-1.0-30	60	51.9	60.0	15.0	30	1.2	400	150	2	15	2	3600	1.0
3600-400-150-1.0-45	60	42.4	60.0	21.2	45	1.2	400	150	2	15	2	3600	1.0
3600-400-150-1.0-60	60	30.0	60.0	25.9	60	1.2	400	150	2	15	2	3600	1.0
3600-400-150-1.0-75	60	15.5	60.0	29.0	75	1.2	400	150	2	15	2	3600	1.0
3600-400-150-1.0-90	60	0.0	60.0	30.0	90	1.2	400	150	2	15	2	3600	1.0

**Table 2** Coupon test results

Specimen details	Young's modulus (N/mm <sup>2</sup> )	Yield stress (N/mm <sup>2</sup> )	Average Young's modulus (N/mm <sup>2</sup> )	Average yield stress (N/mm <sup>2</sup> )
C-1.2-1	$1.99 \times 10^5$	269	$2.04 \times 10^5$	252.00
C-1.2-2	$1.97 \times 10^5$	240		
C-1.2-3	$2.15 \times 10^5$	247		
C-2-1	$2.03 \times 10^5$	262	$2.11 \times 10^5$	247.00
C-2-2	$1.98 \times 10^5$	238		
C-2-3	$2.31 \times 10^5$	241		

The test set-up and testing procedure are followed as reported in Arunkumar and Sukumar [30]. The beams were tested with hinged support at one end and a roller support at the other end. A load cell is used to monitor the applied load. Two-point loads are applied at  $1/3^{\text{rd}}$  distance from each end. Torsion restrained at each end of the specimens by providing lateral supports (clamping arrangement) to the

middle of the web (Fig. 3). Two LVDTs were placed to measure the vertical displacements at mid-span and at one of the loading points. Another LVDT was placed to measure the lateral displacement at mid-span of the top flange lip. The load cell and LVDTs were connected to a data logger to record the readings. The load was applied monotonically with uniform load increments by using

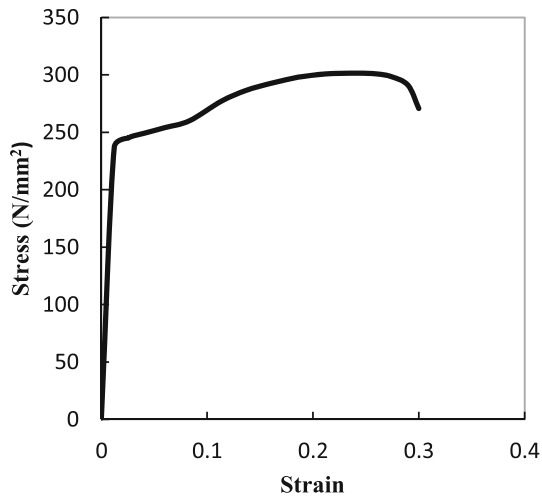
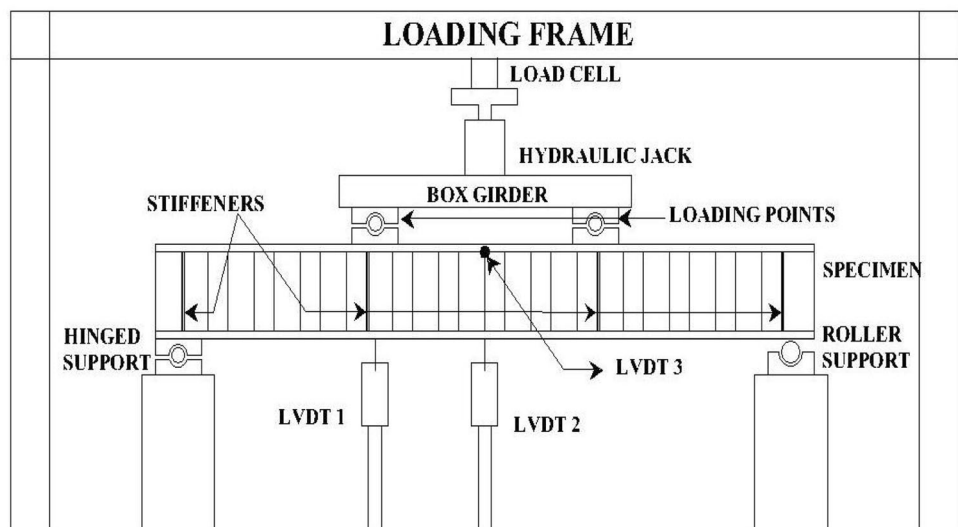


Fig. 2 Stress–strain curve from coupon test



Fig. 3 Experimental set-up

Fig. 4 Schematic diagram of test set-up



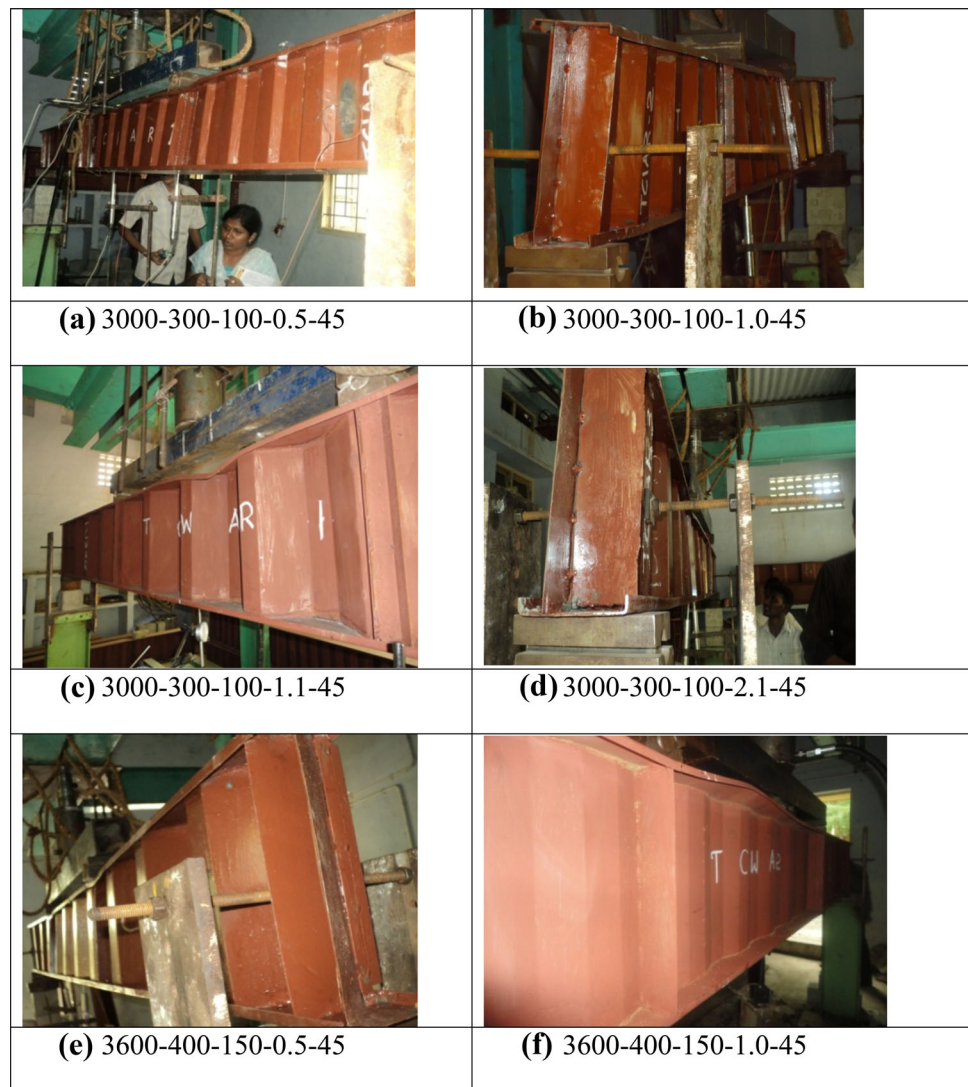
200-kN capacity jack until the specimens reach their unstable position to drop in capacity.

### Results and discussion

The specimens failed by local buckling in the flange region, flange web junction, lateral–torsional buckling and the combination of these failure modes, as shown in Fig. 5, for various specimens. The specimen 3600-400-150-1, which has no corrugation (flat web), failed by shear buckling in the web in the shear zone as shown in Fig. 8a. All other specimens having corrugation in web failed due to local buckling of the compression flange, which led to the failure of lateral–torsional buckling at ultimate load (Fig. 8a).

For 3000-300-100-X-45 series, the aspect ratio varies from 0.47 to 2.1. The moment-carrying capacity is more when the aspect ratio is nearer to 1. 3000-300-100-0.5-45 specimen that failed by initiation of local buckling in the top flange nearer to the loading point in the shear zone and finally failed by lateral buckling of the compression flange. 3000-300-100-0.7-45 and 3000-300-100-1.1-45 specimens failed by local buckling in the top flange nearer to the one of the loading points in the pure bending zone and led to lateral–torsional buckling at failure. 3000-300-100-2.1-45 specimen failed by the initiation of local buckling in top compression flange nearer to two of the loading points in the shear zone simultaneously and led to lateral buckling of the top compression flange at failure. For 3600-400-150-X-45 series, the aspect ratio varied from 0.5 to 2.0 with an increment of 0.5. The moment-carrying capacity is higher when the aspect ratio is 1. 3600-400-150-1.5-45 specimen that failed initially by local buckling in top compression flange in the shear zone and finally lateral buckling of

**Fig. 5** Failure of the various specimens



compression flange that occurred at failure. Remaining three specimens in 3600-400-150-X-45 series failed by initiation of local buckling in top compression flange in the middle of the pure bending zone and finally failed with interaction of lateral buckling of top compression flange. Load versus mid-span deflection curves are plotted for the 3600-400-150-x-45 series specimen. For 1800-200-100-x-45 series, the aspect ratio varied from 0.5 to 2.0 with an increment of 0.5. The moment-carrying capacity is higher when the aspect ratio is 1. 1800-200-100-2.0-45 specimen that failed by initiation of local buckling in top compression flange and led to flexural buckling at failure. Remaining 1800-200-100-x-45 series specimens failed by initiation of local buckling of the web in the shear zone and led to flexure buckling at failure. For 1800-300-100-X-45 series, the aspect ratio varied from 0.5 to 4.0. The moment-carrying capacity is higher when the aspect ratio is 1. In this series, all the specimens failed by initiation of local

buckling near the each loading point in top compression flange and followed by the lateral buckling of the top compression flange. In 1800-300-100-X-45 series, all the five specimens failed by the mixture of local buckling and lateral buckling combination. It is found that when the aspect ratio is 1, the moment capacity is maximum. When the aspect ratio is less than or greater than one, the (unstiffened) flange outstand width on the one side of the web is more while comparing with the section with the aspect ratio one. Hence, the local buckling of the flange occurs earlier in that zone. But, when the aspect ratio is 1, the inclined panel and the horizontal panel width are same and the flange outstand area is the least and the flange is more stiffened than the other, the effective width is more and the local buckling in the compression flange is delayed. From the tests, it is observed that when the aspect ratio is 1, it has more stiffness.

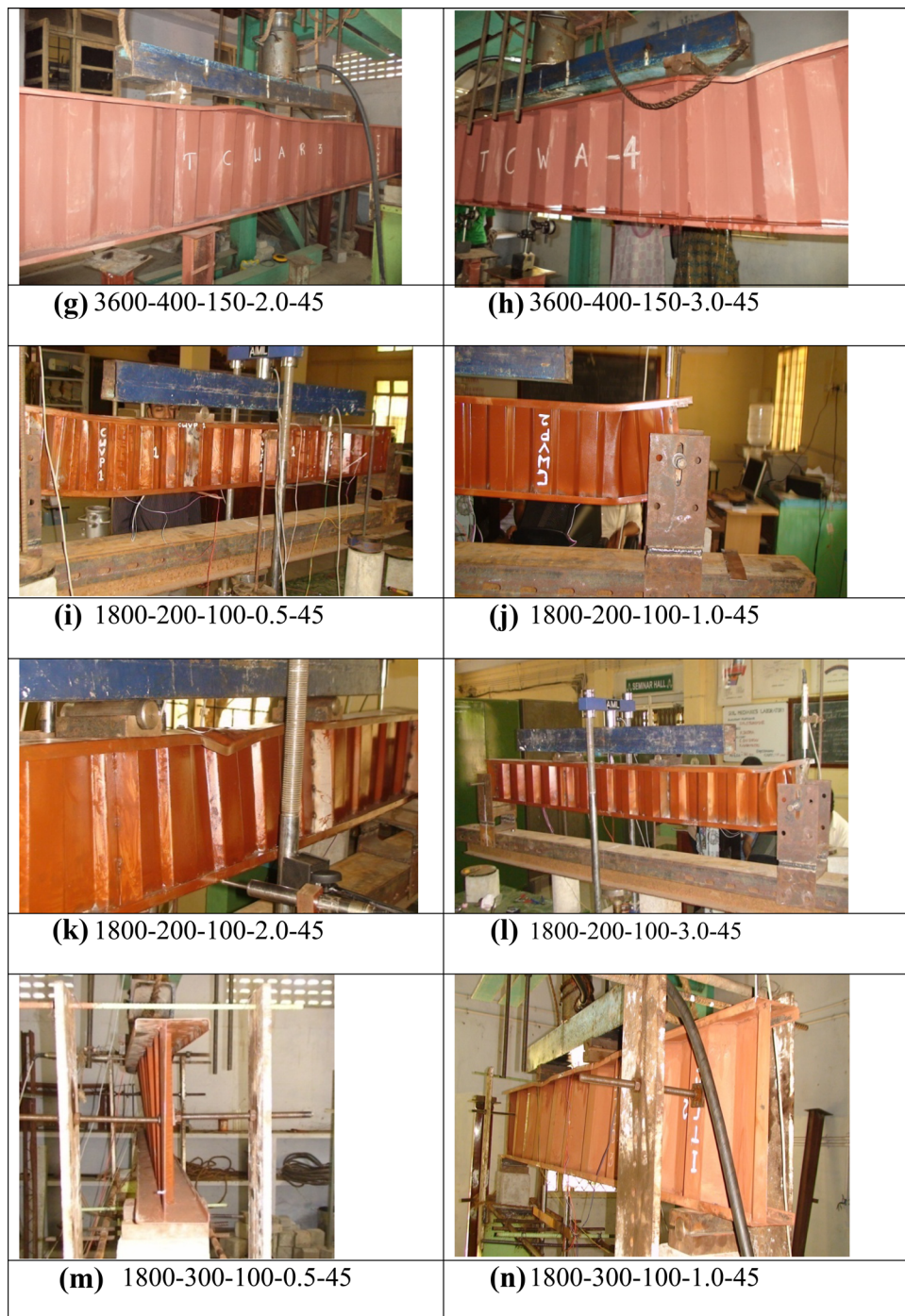


Fig. 5 continued

### Numerical Analysis

Conducting exhaustive experiments involves effort and time. Hence, numerical analysis through finite element softwares gives scope for further studies with proper validation of results with that of experiments [31]. In the present study, ANSYS [25] was used to develop finite

element models, and nonlinear analysis is performed under four-point bending. Centre-line dimensions are used for developing the FE model. Element SHELL 181, which supports nonlinear buckling analyses, is used to develop the proposed finite element model. It is a 4-node element with 6 degrees of freedom at each node: translations in the  $x$ ,  $y$  and  $z$  directions, and rotations about the  $x$ ,  $y$  and  $z$ -axes.



**Fig. 5** continued

In general, it is highly appropriate in linear, large rotation and large strain nonlinear analysis. Totally, 28 FE models were developed corresponding to the respective tested specimens. Through the convergence study (results shown in Table 3), an approximate mesh size of 20 mm  $\times$  20 mm for flange and web and 20 mm  $\times$  15 mm for lip was adopted for this study. Residual stress and effect of cold-forming process are not included in the FE model. Initial imperfections are incorporated by scaling the buckling modes through eigenvalue analysis as proposed by Schafer and Pekoz [32]. As there were no welded connection failure observed in all specimens during the experiments, the weld joint between the plate components was simulated through coupling constraints. Nonlinear material properties

are incorporated with the results obtained from the tension coupon tests. Thus, geometric and material nonlinearities are incorporated in the FE model. Appropriate boundary conditions to simulate simply supported boundary condition by restraining  $u_x$ ,  $u_y$ ,  $u_z$  at one end (pin support) and  $u_x$  and  $u_y$  at the other end (roller support) were assigned as shown in Fig. 6 [33]. At the centre node of the web of the support,  $u_x$  and  $\theta_x$  were restrained to simulate the lateral clamping provided in the test set-up. The application of loads and boundary conditions in the finite element model is shown in Fig. 6. The load was applied to the set of nodes at two loading points of the beam as shown in Fig. 6. The nonlinear finite element analysis was performed with the incremental-iterative technique, which combines the



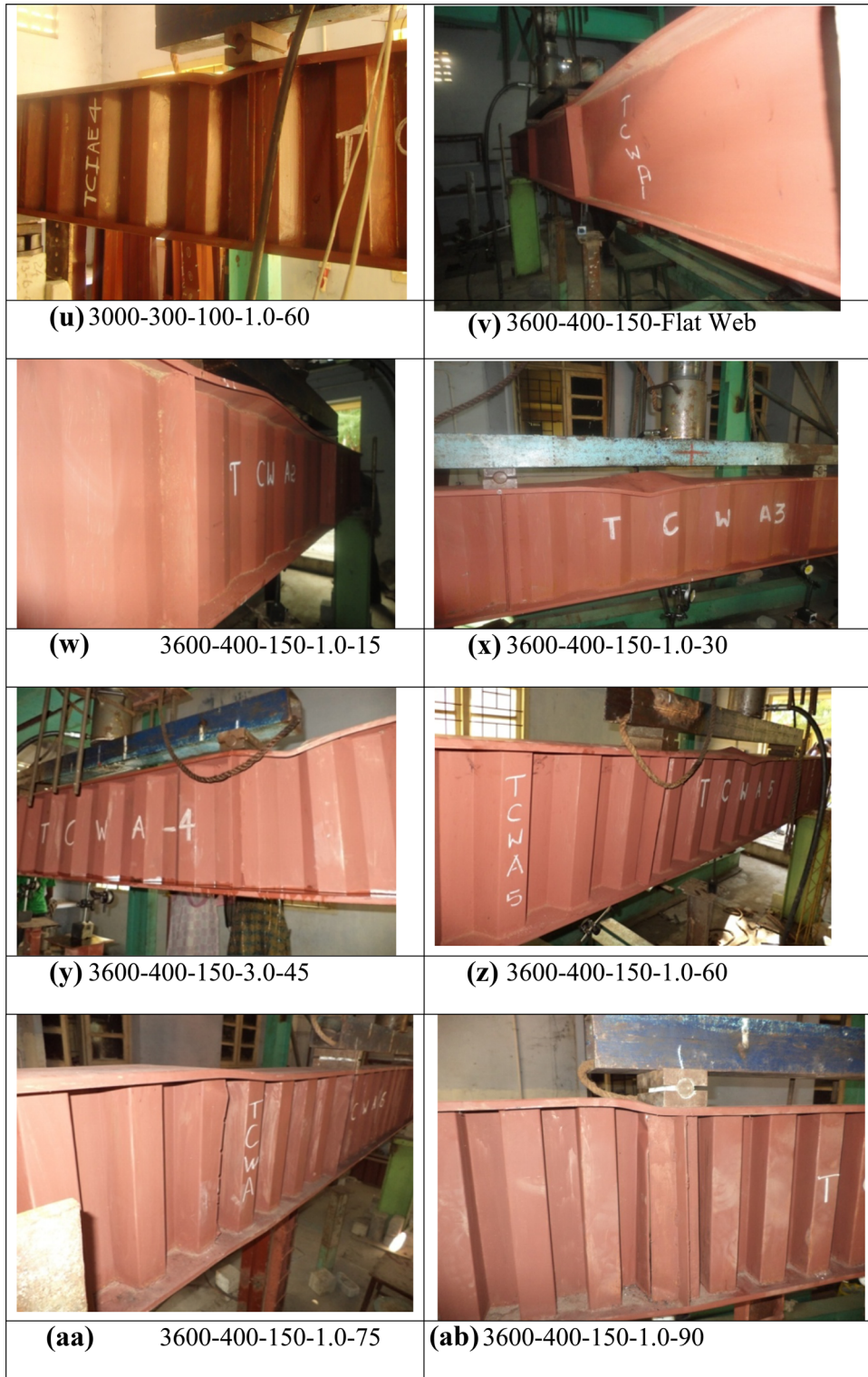


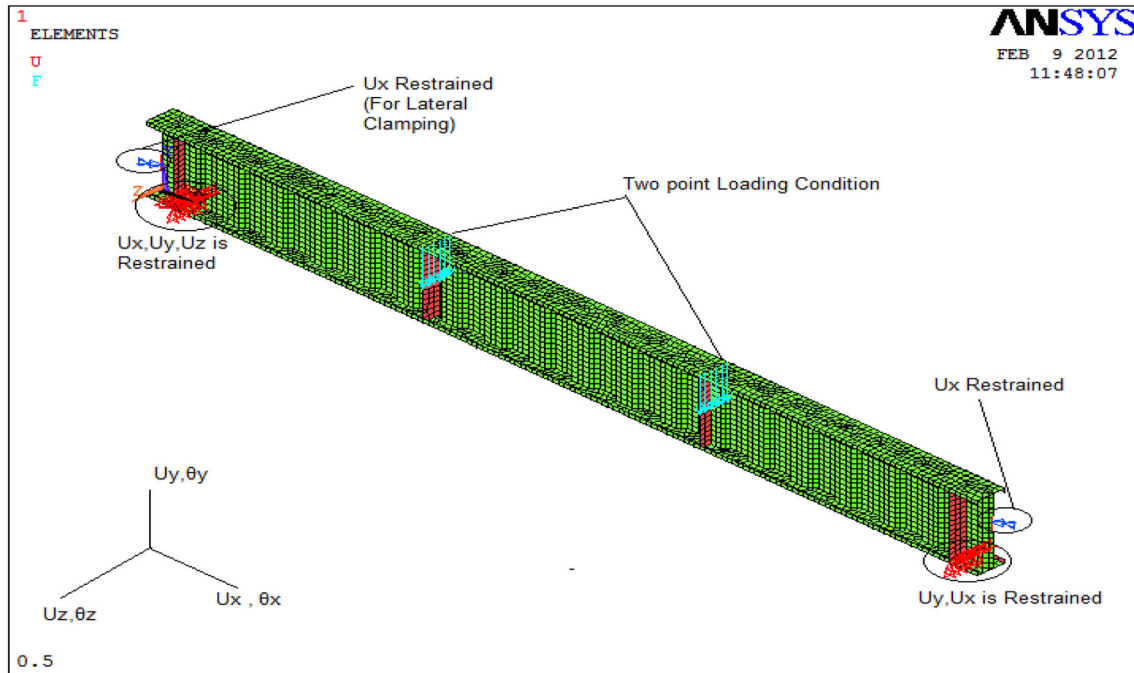
**Fig. 5** continued

Newton–Raphson method and the arc-length control method. The results obtained from FE models are

compared in terms of load–deflection response and failure modes.

**Table 3** Results of mesh convergence study

Specimen ID	Moment (kN m)				
	Test	FEA			
		20 mm	15 mm	10 mm	5 mm
3000-300-100-0.5-45	14.06	13.66	15.74	15.77	16.02
3600-400-150-0.5-45	27.56	24.80	29.83	29.96	30.21
1800-200-100-0.5-45	11.67	11.84	12.75	12.96	13.28
1800-300-100-0.5-45	15.70	15.40	16.57	16.84	17.01

**Fig. 6** Load and boundary condition of FE model

### Verification of FE Model

The results obtained from the FE model are compared in terms of load versus deflection curves and failure modes. A typical comparison of load–deflection curves of two FE models corresponding to the 3600-400-150-Flat Web and 3600-400-150-1.0-45 is shown in Fig. 7a, b, respectively. It is found that the predicted load–deflection curve is closely matched with the experimental curves. Further, the failures predicted by the FE model are also matching close to that obtained experiments. A typical comparison of failure modes is shown in Fig. 8a and b. The FE model corresponding to the specimen, TCA-3600-400-150-1, predicts the failure by shear buckling between the stiffeners as observed in experiments. The corrugated specimen, TCA-3600-400-150-5, failed by buckling of the compression flange in the constant moment region, which is also

obtained from the corresponding FE model as shown in Fig. 8b.

Comparison of the ultimate moment obtained from FEA and experiment with that obtained from codes of practices, such as Australian/New Zealand Standards [27] and North American Specifications [26], is given in Table 3. The moment capacity obtained from FEA and codes of practices is normalized with that obtained from experiments. Table 4 compares that the moment capacities ( $M_{FEA}$ ) predicted by FEA are compared with experimental moment capacities ( $M_{Exp}$ ) with the mean and standard deviation of the ratio of test to FEA ultimate moment resistances, which are 0.93 and 0.08, respectively, which shows reasonable agreement.

**Table 4** Comparison of results

Specimen ID	$M_{Exp}$ (kNm)	$M_{FEA}$ (kNm)	$M_{AISI}$ (kNm)	$M_{As/Nz}$ (kNm)	$M_{FEA}/M_{Exp}$	$M_{AISI}/M_{Exp}$	$M_{As/Nz}/M_{Exp}$
3000-300-100-0.5-45	14.06	13.66	13.74	13.77	0.97	0.98	0.98
3000-300-100-0.7-45	14.91	14.16	14.00	13.90	0.95	0.94	0.93
3000-300-100-1.1-45	16.82	16.17	14.32	14.06	0.96	0.85	0.84
3000-300-100-2.1-45	15.62	15.66	14.65	14.24	1.00	0.94	0.91
3600-400-150-0.5-45	27.56	24.80	26.83	25.76	0.90	0.97	0.93
3600-400-150-1.0-45	28.71	27.20	26.94	26.07	0.95	0.94	0.91
3600-400-150-1.5-45	26.54	23.07	26.33	25.47	0.87	0.99	0.96
3600-400-150-2.0-45	25.99	22.56	25.51	24.77	0.87	0.98	0.95
1800-200-100-0.5-45	11.67	11.84	12.00	12.12	1.01	1.03	1.04
1800-200-100-1.0-45	12.07	12.49	12.00	12.12	1.03	0.99	1.00
1800-200-100-2.0-45	11.62	11.41	12.00	12.12	0.98	1.03	1.04
1800-200-100-3.0-45	11.37	11.26	12.00	12.12	0.99	1.06	1.07
1800-300-100-0.5-45	15.70	15.40	16.57	16.57	0.98	1.06	1.06
1800-300-100-1.0-45	16.48	16.17	16.57	16.57	0.98	1.01	1.01
1800-300-100-2.0-45	15.94	15.67	16.57	16.57	0.98	1.04	1.04
1800-300-100-3.0-45	15.86	15.53	16.57	16.57	0.98	1.04	1.04
1800-300-100-4.0-45	15.43	15.36	16.57	16.57	1.00	1.07	1.07
3000-300-100-1.0-15	14.90	11.70	13.70	13.67	0.79	0.92	0.92
3000-300-100-1.0-30	16.20	12.21	13.86	13.77	0.75	0.86	0.85
3000-300-100-1.0-45	16.82	13.45	14.19	14.05	0.80	0.84	0.84
3000-300-100-1.0-60	18.05	13.57	14.04	13.91	0.75	0.78	0.77
3600-400-150-Flat web	25.06	21.74	24.23	24.75	0.87	0.97	0.99
3600-400-150-1.0-15	26.24	22.31	26.72	25.92	0.85	1.02	0.99
3600-400-150-1.0-30	27.14	23.89	26.82	25.98	0.88	0.99	0.96
3600-400-150-1.0-45	28.71	27.20	26.94	26.07	0.95	0.94	0.91
3600-400-150-1.0-60	31.32	29.13	27.04	26.17	0.93	0.86	0.84
3600-400-150-1.0-75	32.36	30.96	27.10	26.23	0.96	0.84	0.81
3600-400-150-1.0-90	32.89	33.56	27.13	26.26	1.02	0.82	0.80
Mean					0.93	0.96	0.95
SD					0.08	0.08	0.09
Capacity reduction factor ( $\varphi$ )						0.9	0.9
Reliability index ( $\beta$ )						2.74	2.77

**Theoretical Analysis**

No specific design rules are available in Australian/New Zealand Standards [27] and North American Specifications [26] for calculating the moment-carrying capacity of I-section with trapezoidal corrugated web. In this, properties such as the polar radius of gyration of the cross section about the centre, radius of gyration, section modulus, and warping constant vary along the longitudinal direction due to a change in depth of corrugation ‘d’, which results in change in the properties. Due to changes in depth of corrugation ‘d’, along the length of the member, a position of centroidal y-axis also changes along the length and the geometric properties are not constant at all sections. In order to find lateral buckling moment capacity, elastic

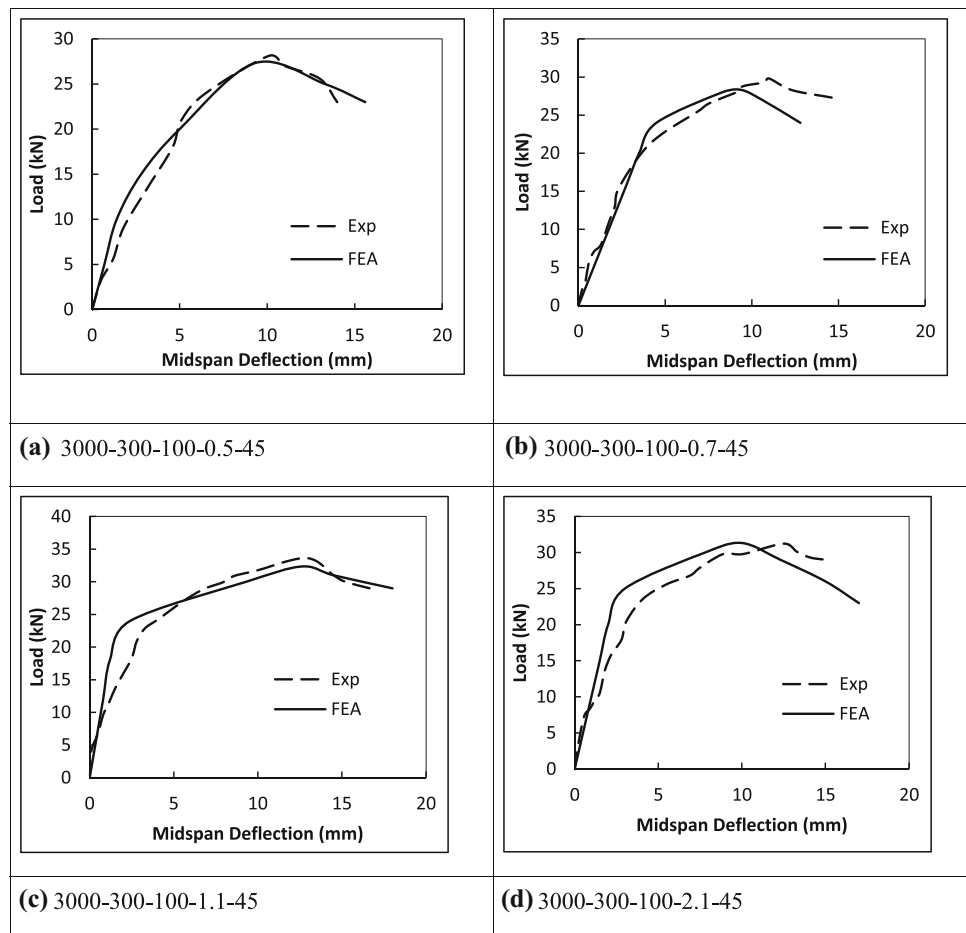
buckling stress for flexural buckling about the y-axis  $f_{oy}$  and elastic buckling stress for torsional buckling  $f_{oz}$  have to be calculated. Hence, to find lateral buckling strength, a new value  $d_{avg}$  is calculated as suggested by Moon et al. [18, 19] in Eq. (1).

$$d_{avg} = [(2a + b) * d_{max}] / [2 * (a + b)] \tag{1}$$

**Comparison of results**

The theoretical results are presented and compared with experimental and numerical results (Table 3). The predominant mode of failure in all the specimens in both Australian/New Zealand Standards [27]) and North American Specifications (NAS) [26] is lateral–torsional

**Fig. 7** Comparison of result for load versus deflection curve for FEA and experiment



buckling. The mean values of the  $M_{FEA}/M_{Exp}$ ,  $M_{AISI}/M_{Exp}$  and  $M_{AS/NZ}/M_{Exp}$  are 0.93, 0.96 and 0.95 with a standard deviation of 0.08, 0.08 and 0.09, respectively. The reliability analysis followed in this study as reported by Anbarasu [3, 34]. The reliability index for the current Australian/ New Zealand Standards [27] and North American Specifications [26] is 2.74 and 2.77, respectively. It is found that the code results are conservative and reliable.

The test moment and FEA moments are plotted against the aspect ratio (Fig. 9). It is found that moment capacity calculated in the FEA follows the same trend with the experiment. For more depth of web, the difference between FEA result and the experimental result is found to be little higher. From the figure, it is evident that the moment capacity reaches a maximum when the aspect ratio is nearly one. It is because when the aspect ratio is less than one (the horizontal panels are wider than the inclined panels) the horizontal panels are slender and weaker, which governs the failure. On the other hand, for aspect ratio greater than one (the inclined panels are wider than the horizontal panels), the inclined panels are slender and weaker, which governs the failure. When the aspect ratio is

one (the horizontal panels and inclined panels are equal), both panels have the same slenderness and failure is equally possible in either panels, and hence, the flexural capacity is higher when the aspect ratio is one. When the aspect ratio is more than one, the unstiffened outstand area is more; there is a possibility of initiation of failure in the unstiffened area; hence, beyond this aspect ratio 1 effective width will not increase and hence there is no increase in moment capacity.

The test moment and FEA moment are plotted against the corrugation angle (degrees) (Fig. 10). It is found that moment capacity in FEA is quite closer to experimental moment capacity. From the figure, it is observed that moment capacity increases with the increase in corrugation angle for both the series of the specimen. The increase in corrugation angle increases the depth of corrugation or the flange outstand on one side, which in turn increases the moment of inertia about the minor axis ( $I_y$ ). This increase in the moment of inertia about the minor axis ( $I_y$ ) increases the resistance to the lateral–torsional buckling that is why the moment capacity increases with the increase in corrugation angle. But, the increase in corrugation angle more than  $60^\circ$  shows less increase in moment capacity. This is

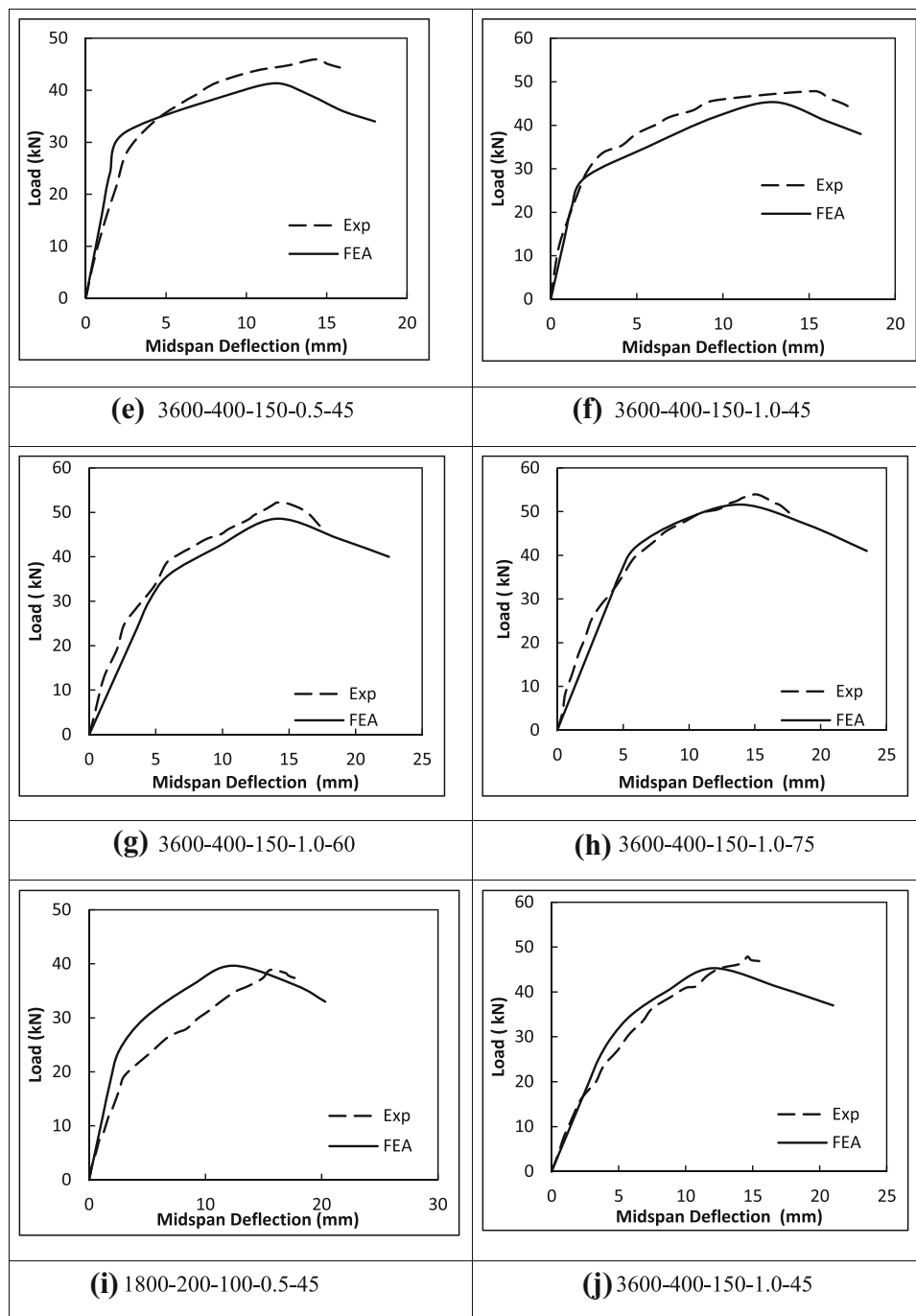
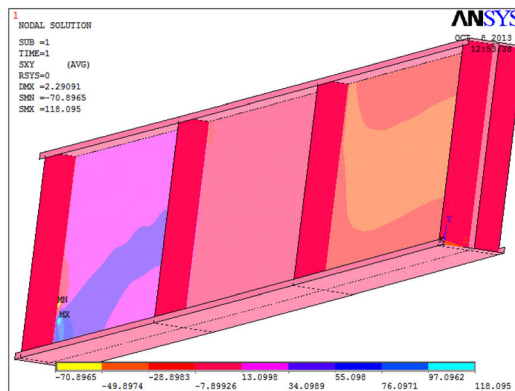


Fig. 7 continued

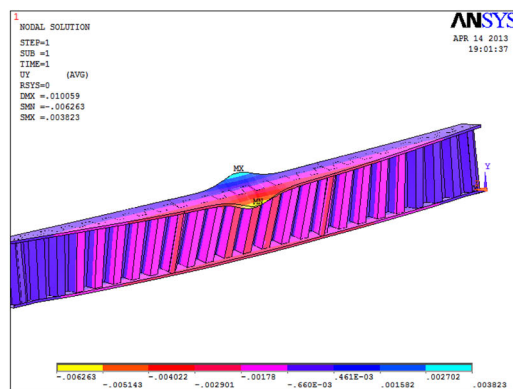
because the increase in corrugation angle increases the flange outstand on one side, which decreases the effective width of the flange. Therefore, further improvement in moment capacity is less. So increase in corrugation angle beyond 60° does not show any notable increase in the moment capacity.

### Conclusion

An experimental investigation for the cold-formed built-up I-section with corrugated web was presented in this paper. Initially, a total of 28 built-up I-section corrugated web beams were tested under the simply supported end condition. The cross-sectional dimension, the corrugation angle,



(a) For specimen 3600-400-150-Flat Web



(b) For specimen of 3600-400-1.0-60

Fig. 8 Comparison of experimental and FEA failure mode

aspect ratio, thickness and the length of the test members were varied in the tests to find its influence on the flexural capacity of the beam. Simply supported beams were tested under four-point bending about the major axis of the sections. The moment resistance capacities and the failure modes were reported. It is found that flexural capacity is more when the aspect ratio is nearer to one. It is found that moment capacity increases with the increase in corrugation angle up to 60°. Further increase in corrugation angle beyond 60° results in a meagre increase in the flexural capacity. In addition, a nonlinear finite element model was developed and validated against the experimental results. The moment capacities of the tested cold-formed steel built-up I-section with corrugated web were compared with the finite element analysis results and the nominal moment capacities predicted by using the current specifications in AS/NZS and NAS for cold-formed steel structures. Moment capacity of corrugated web is more compared to the flat web, and shear failure is eliminated due to corrugations in the web. The mean and standard deviation for the moment capacity of experiment to North American

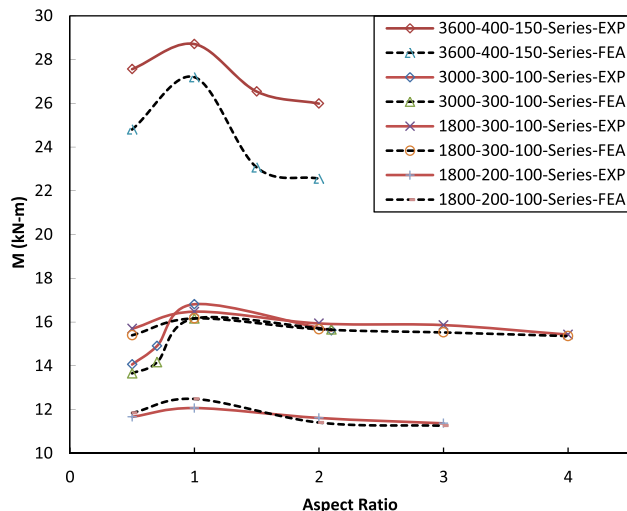
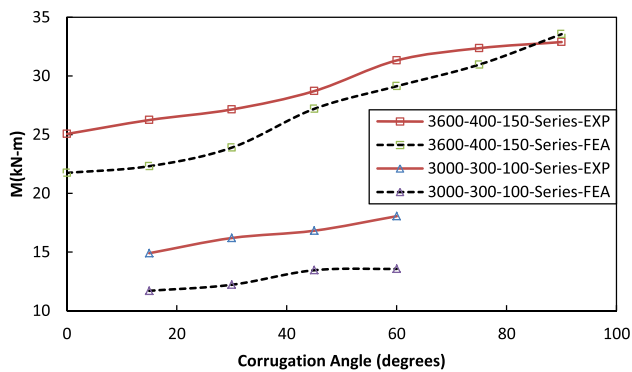


Fig. 9 Ultimate moment versus aspect ratio



**Fig. 10** Ultimate moment versus corrugation angle

Specifications (AISI S100-2007) ratio are 1.05 and 0.09, respectively. The mean and standard deviation for the moment capacity of experiment to Australian/New Zealand Standards (AS/NZS 4600:2005) ratio are 1.07 and 0.10, respectively. It is showed that the nominal moment capacities predicted using both the current specifications are quite conservative for the cold-formed steel built-up I-beam with corrugation in the web subjected to bending, especially for those specimens failed by lateral–torsional buckling. Local buckling on the compression flange, which initiates the failure, may be due to unstiffened outstand area on one side, which is more due to trapezoidal corrugation. The effective width will be less even though width is more in order to resist the compression in the top flange of the beam. Furthermore, the reliability analysis demonstrated that both the design specifications are reliable when the resistance factor ( $\phi$ ) of 0.9 was used.

**Funding** There was no funding received for this research.

**Declaration**

**Conflict of interest** On behalf of all authors, the corresponding author states that there is no conflict of interest.

## References

- J.K. Sonu, K.D. Singh, Shear behavior of stiffened single perforated lean duplex stainless steel (LDSS) rectangular hollow beams. *J. Constr. Steel Res.* **176**, 106377 (2021)
- S. Selvaraj, M. Madhavan, Structural design of cold-formed steel face-to-face connected built-up beams using direct strength method. *J. Constr. Steel Res.* **160**, 613–628 (2019)
- M. Anbarasu, Simulation of flexural behaviour and design of cold-formed steel closed built-up beams composed of two sigma sections for local buckling. *Eng. Struct.* **191**, 549–562 (2019)
- K. Aggarwal, J. Papangelis, S. Wu, Finite element analysis of local shear buckling in corrugated web beams. *Eng. Struct.* **162**, 37–50 (2018)
- M.A. Dar, N. Subramanian, A.R. Dar, M. Muheeb, M. Haseeb, T. Mugees, Structural efficiency of various strengthening schemes for cold-formed steel beams: effect of global imperfections. *Steel Compos. Struct.* **30**(4), 393–403 (2019)
- M. Zhou, X.N. Shang, M.F. Hassanein, L.Y. Zhou, The differences in the mechanical performance of prismatic and non-prismatic beams with corrugated steel webs: a comparative research. *Thin-Walled Struct.* **141**, 40–410 (2019)
- M. Elchalakani, A.A. Elkawas, M.F. Hassanein, Lateraltorsional buckling strength and behaviour of high-strength steel corrugated web girders for bridge construction. *Thin-Walled Struct.* **122**, 112–123 (2018)
- D. Sherman, J. Fisher, Beams with corrugated webs. In: Proceedings of the 1st International Specialty Conference on Cold-Formed Steel Structures. Missouri-Rolla, pp. 198–204 (1971)
- J. Lindner. Lateral-Torsional buckling of beams with trapezoidally corrugated webs. In: Proceedings of the 4th international colloquium on stability of steel structures. Budapest, Hungary, pp. 305–308 (1990).
- R. Luo, B. Edlund, Ultimate strength of girders with trapezoidally corrugated webs under patch loading. *Thin-Walled Struct.* **24**, 135–156 (1996)
- M. Elgaaly et al., Shear strength of Beams with corrugated webs. *J. Struct. Eng. ASCE* **122**(4), 390–398 (1996)
- M. Elgaaly et al., Bending strength of steel beams with corrugated webs. *J. Struct. Eng. ASCE* **123**(6), 772–782 (1997)
- M. Elgaaly, A. Seshadi, Girders with corrugated webs under partial compressive edge loading. *J. Struct. Eng. ASCE* **123**(6), 783–791 (1997)
- Y.A. Khalid et al., Bending behavior of corrugated web beams. *J. Mater. Process. Technol.* **150**, 242–254 (2004)
- E.Y. Sayed-Ahmed, Plate Girders with corrugated steel webs. *AISC Eng. J.* **42**, 111–123 (2005)
- H.H. Abbas, R. Sause, R.G. Driver, Analysis of flange transverse bending of corrugated web I-girders under in-plane loads. *J. Struct. Eng. ASCE* **133**(3), 347–355 (2007)
- E.Y. Sayed-Ahmed, Design aspects of steel I-girders with corrugated steel webs. *Electron. J. Struct. Eng.* **7**, 27–40 (2007)
- J. Moon et al., Lateral torsion-flexure buckling of I-girder with corrugated webs under uniform bending. *Thin-Walled Struct.* **47**, 21–30 (2009a)
- J. Moon et al., Shear Strength and design of trapezoidally corrugated webs. *J. Constr. Steel Res.* **65**, 1198–1205 (2009b)
- J. He et al., Mechanical behavior and analysis of composite bridges with corrugated steel webs. *Int. J. Steel Struct.* **12**(3), 321–338 (2012)
- Zs. Nagy et al., Romanian application of cold-formed steel beams with screwed corrugated webs. *Steel Constr.* **6**(2), 139–143 (2013)
- D. Dubina et al., Cold-formed steel beams with corrugated web and discrete web-to-flange fasteners. *Steel Constr.* **6**(2), 74–81 (2013)
- D. Dubina et al., Experimental investigations of cold-formed steel beams of corrugated web and built-up section for flanges. *Thin-Walled Struct.* **90**, 159–170 (2015)
- R.I. Ballok. Structural systems with trapezoidal beams made of cold-formed steel profiles and corrugated web. PhD Thesis, Technical University of Cluj-Napoca, Romania (2014).
- ANSYS, version 12.0. (2009) Finite Element Analysis Software. ANSYS.INC.
- AISI-S100 (2007) North American specification for the design of cold-formed steel structural members specifications. Washington, DC, U.S.A.
- AS/NZ: 4600 (2005) Australian/New Zealand Standard—Cold-formed steel structures

28. IS 1608. (2005) (Part-I) Metallic materials—tensile testing at ambient temperature
29. J. Yan, B. Young, Column tests of cold-formed steel channels with complex stiffeners. *J. Struct. Eng.* **128**, 737–745 (2002)
30. G. Arunkumar, S. Sukumar, A simplified method for calculating warping constant for lipped I-beam with trapezoidal corrugation in web. *J. Struct. Eng. (madras)* **40**(6), 546–557 (2014)
31. M. Anbarasu, A numerical investigation of local–distortional–lateral-torsional buckling interaction of cold-formed steel lipped channel beams. *Asian J. Civ. Eng. (BHRC)* **18**(4), 643–656 (2017)
32. B.W. Schafer, T. Pekoz, Computational modelling of cold-formed steel: characterizing geometric imperfections and residual stress. *J. Constr. Steel Res.* **47**, 193–210 (1998)
33. C.W. Kurniawa, M. Mahendran, Elastic lateral buckling of cantilevered lite steel beams under transverse loading. *Int. J. Steel Struct.* **11**(4), 395–408 (2011)
34. M. Anbarasu, Local-distortional buckling interaction on cold-formed steel lipped channel beams. *Thin-Walled Struct.* **98**, 351–359 (2016)

**Publisher's Note** Springer Nature remains neutral with regard to jurisdictional claims in published maps and institutional affiliations.